Occultation Experiment: Results of the First Direct Measurement of Mars's Atmosphere and Ionosphere

Abstract. *Changes in the frequency, phase, and amplitude of the Mariner IV radio signal, caused by passage through the atmosphere and ionosphere of Mars, were observed immediately before and after occultation by the planet. Preliminary analysis of these effects has yielded estimates of the refractivity and density of the atmosphere near the surface, the scale height in the atmosphere, and the electron density profile of the Martian ionosphere. The atmospheric density, temperature, and scale height are lower than previously predicted, as are the maximum density, temperature, scale height, and altitude of the ionosphere.*

Approximately 1 hour after its closest approach to Mars on 15 July 1965, the Mariner IV spacecraft disappeared beyond the limb of the planet, as seen from Earth, and remained in occultation for approximately 54 minutes. Immediately prior to the beginning and immediately after the end of occultation, the spacecraft's S-band radio signal passed through the atmosphere and ionosphere of Mars, both on its way up to the spacecraft, and on its way to Earth after being coherently retransmitted. When this signal reached Earth about 12 minutes later, it marked the first time that a coherent radio transmission has been used to probe the atmosphere and ionosphere of another planet. The changes in frequency, phase, and amplitude of the signal caused by passage through these media have provided new information on the physical properties of the Martian atmosphere and ionosphere.

The acquisition of information to improve the knowledge of the Martian environment has been the objective of the Mariner IV occultation experiment (*1*). Previous knowledge of such atmospheric properties as the surface pressure and density, as well as scale height, is quite poorly defined. The surface pressure, as deduced from recent spectroscopic observations of weak and strong CO_2 absorption bands, was thought to lie somewhere between 10 and 40 mb (*2*). The vertical structure of the atmosphere has not previously been accessible to direct Earth-based measurement and it could only be estimated on the basis of assumption of atmospheric constituents and temperatures. Similarly, the properties of the Martian ionosphere have been the subject of speculation based on the estimated structure of the Martian upper atmosphere, with some models indicating an expected peak electron density of 10^5 to 2×10^7 electrons per cubic centimeter (*3*).

The results of the Mariner IV occultation experiment, when fully analyzed, will provide an improved definition of the surface density and pressure, as well as of the vertical structure of the atmosphere and the electron density profile of the ionosphere, of Mars. However, even a rather superficial analysis, performed in the time since acquisition of the data on 15 July, has yielded significant results.

As the spacecraft approached the limb of the planet, the presence of an atmosphere and ionosphere caused the velocity of propagation of the radio signal to deviate from that in free space because of the nonunity index of refraction of the neutral and ionized media. Also, the radial gradient of the effective index of refraction caused the radio beam to be refracted from a straight-line path. Both of these effects caused the phase-path length of the propagation to differ from what would have been observed in the absence of an atmosphere and ionosphere. Thus, since the geometry obtained from the estimated trajectory is known, the measured deviation in phase can be used to estimate the spatial characteristics of the index of refraction (or refractivity) in the atmosphere and ionosphere by a process of integral inversion or by model fitting (*4, 5*).

The analysis of Doppler tracking data taken before and after planetary encounter yields the trajectory of the spacecraft at the time of occultation with such precision that the range rate of the spacecraft is known to an accuracy of 0.0015 m/sec. Thus, any significant deviation of the received Doppler data from predictions based on trajectory analysis can be expected to have been caused by atmospheric and ionospheric phase-path effects.

It must be pointed out that the phase changes due to the atmosphere amount to about 30 cycles (wavelengths), and those due to the ionosphere about 10 cycles. They are obtained by subtracting, from the total radio-frequency phase change of about 3×10^{11} cycles during the time period of the experiment, all the predictable phase shift caused by the motion of the spacecraft, reference phase changes, motion of the stations on Earth (3×10^7 cycles), light-transit time effects, the effects of Earth's troposphere, and others. Thus, it is implied that the total phase change due to all causes other than the atmosphere and ionsophere of Mars must be known to an accuracy of less than 1 part in 10^{11}.

Before discussing the data obtained in this manner, we will describe the geometry of occultation for both entry and exit. At entry into occultation, the spacecraft was at a distance of 25,570 km from the limb of Mars, traveling at a velocity of 2.07 km/sec normal to the Earth-Mars line. The point of tangency on the surface of Mars was at a latitude of 55°S and a longitude of 177°E, corresponding to a point between Electris and Mare Chronium. At the time of exit from occultation, the distance from the limb of Mars had increased to 39,130 km, and the point of tangency was located at about 60°N and 34°W, falling within Mare Acidalium.

Doppler and amplitude data were taken both during entry and exit by the NASA/JPL Deep Space Instrumentation Facilities (DSIF) at Goldstone, California, and Tidbinbilla and Woomera, Australia. The Goldstone stations (Echo and Pioneer) took standard tracking Doppler (closed-loop) as well as open-loop records (described below) of the received signal. The Australian stations took only Doppler data. At entry all data were taken while the spacecraft's transmitter frequency reference was provided by a frequency standard on Earth. At exit, a portion of the data was received while the spacecraft's transmitter frequency reference was provided by an on-board crystal oscillator. In the latter mode, the precision of phase measurements is significantly degraded.

Figure 1 shows the observed minus the predicted phase change in 1 second based on data received at the various DSIF stations. The points marked O/L have been obtained from the open-loop records by means of spectral density analysis, and the other points are derived directly from data processed through the JPL orbit-determination

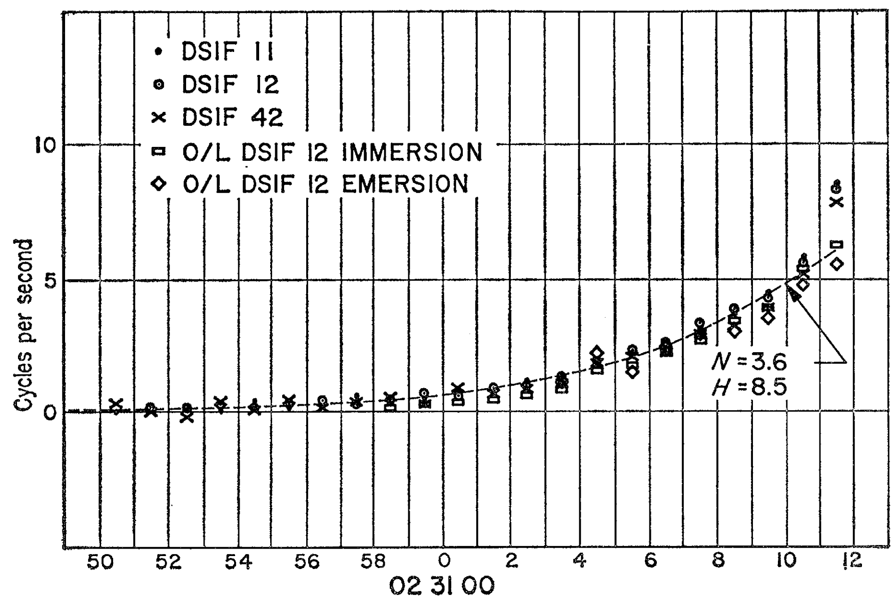

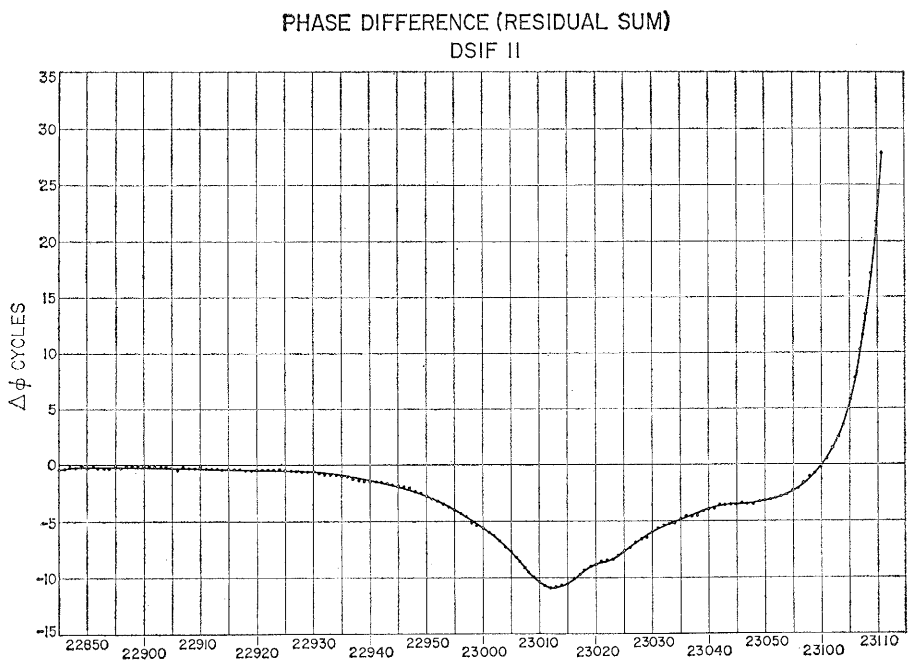

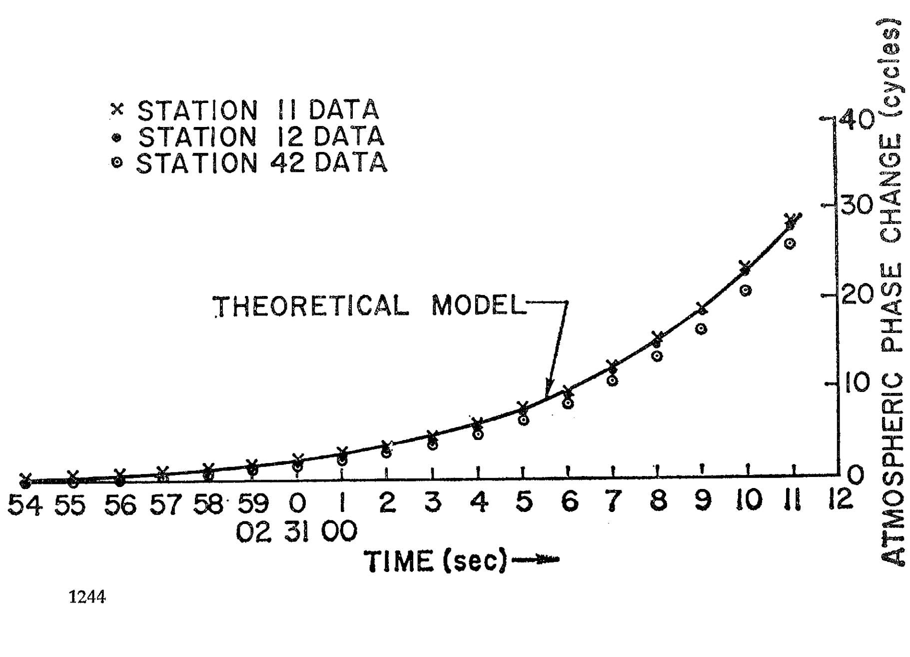

Fig. 1 (top). Doppler residuals. The observed minus the predicted phase changes in 1 second. Abscissa is U.T. 15 July. Fig. 2 (center). Relation of total phase change to time. Abscissa is U.T. 15 July. Fig. 3 (bottom). Portion of graph of Fig. 2 in neutral atmosphere.

program. One may observe that the data from the various sources show a high degree of consistency, except for the Doppler points at 02:31:11.5, which are suspect because the time of loss of signal is estimated to be between 02:31:11.2 and 02:31:11.6 U.T.

A different presentation is shown in Fig. 2, which represents the total phase change as a function of time, derived from station 11 (Goldstone-Pioneer) Doppler residuals. The maximum effect of the ionosphere appears at about 02:30:10, and the final upswing, beginning at about 02:30:50, is caused by the neutral atmosphere. It is interesting to note the extreme smoothness of data suggested by the low scatter of the points.

An expanded portion of the phase-change plot is shown in Fig. 3. This graph relates only to the neutral atmosphere, as the effects of the ionosphere have been removed. Signal extinction time is assumed as 02:31:11.2.

The solid curve represents the computed phase change for a theoretical exponential model atmosphere having a surface refractivity (N) of 3.7 N units and a scale height of 9 km. Even with this relatively crude model the fit is excellent. The dotted line in Fig. 1 represents the computed Doppler residuals for a similar model atmosphere, having a scale height of 8.5 km and N = 3.6. As in the case of the phase change, the fit of the data appears to be quite good.

Figure 4 relates maximum phase change, maximum frequency change (Doppler), and refractive gain (at the time of extinction of the signal of 02:31:11.2) to the surface refractivity and scale height of an exponential density model of an atmosphere. Suggested values of 5.5 ± 0.5 cy/sec, 29 ± 2 cy, and 1.5 to 2.0 db lead to the stippled area in the figure. This area corresponds to a surface refractivity of 3.6 ± 0.2 N units and a scale height of 9 ± 1 km. The gain figure is least reliable, but it can be seen that better values from detailed analysis of data from all the stations should help considerably in reducing uncertainty. In addition, the

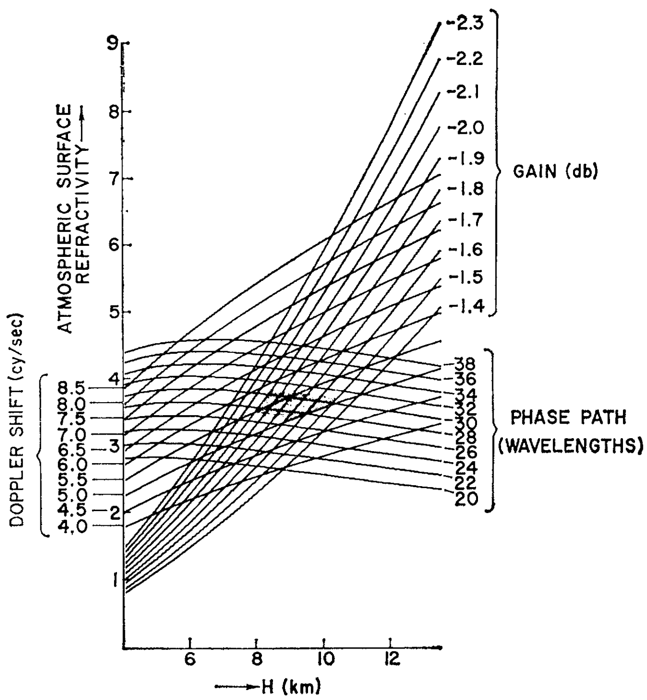

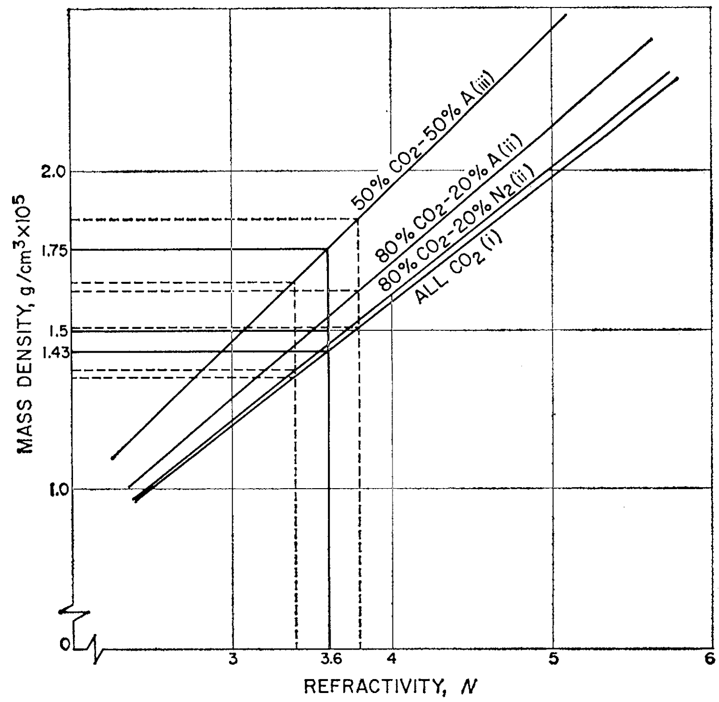

Fig. 4 (left). Maximum changes of phase and frequency in relation to refractivity and scale height of model atmospheres. Fig. 5 (right). Refractivity and mass density as a function of atmosphere composition.

measurements of the Fresnel diffraction pattern should provide an independent set of contours parallel to the gain curves for further refinement (*5*).

A cursory study of the Fresnel pattern in the amplitude recordings leads us to believe that signal dropout was due to a diffracting edge, establishing the very important fact that the final ray paths grazed a surface feature on Mars. All references to surface conditions in this report refer to the altitude of this surface feature. We do not know, of course, its altitude relative to the mean surface of Mars, but the geometry of the experiment would make it likely that it was higher than the mean surface. The mean surface density and pressure would be about 1 percent larger than the values given here for each 90 m of height of the occulting feature above the mean surface level.

So far, analysis shows no obvious change of scale height with altitude to about 30 km.

In essence then, a simple refractivity model of the Martian atmosphere has been established. It now remains to infer density and pressure, thus bringing into focus the question of composition and temperature.

Figure 5 shows the relation between refractivity and mass density as a function of composition, ranging from pure CO_2 to 50 percent CO_2 and 50 percent argon. Since the Martian atmosphere contains spectroscopically measurable amounts of CO_2, and the scale height has been established to about 8 to 10 km, it can be reasonably assumed that the atmosphere consists primarily of CO_2.

Three models differing in composition are considered here: (i) pure CO_2; (ii) 80 to 100 percent CO_2 and the rest argon or nitrogen, in any proportion; and (iii) 50 percent CO_2 and 50 percent argon.

For the atmosphere composed of pure CO_2 (model i) the total number density at the surface, corresponding to the measured refractivity values stated above, was about $1.9 \pm 0.1 \times 10^{17}$ molecules per cubic centimeter (mol/cm^3). The mass density (Fig. 5) is then about $1.43 \pm 0.10 \times 10^{-5}$ g/cm^3. From the measured value of scale height, the temperature range would have to be about 180° ± 20°K, leading to a surface pressure range of 4.1 to 5.7 mb.

For atmosphere model ii (80 to 100 percent CO_2), the number and mass densities are $2.1 \pm 0.2 \times 10^{17}$ mol/cm^3 and $1.5 \pm 0.15 \times 10^{-5}$ g/cm^3, respectively. From the assumed percentage

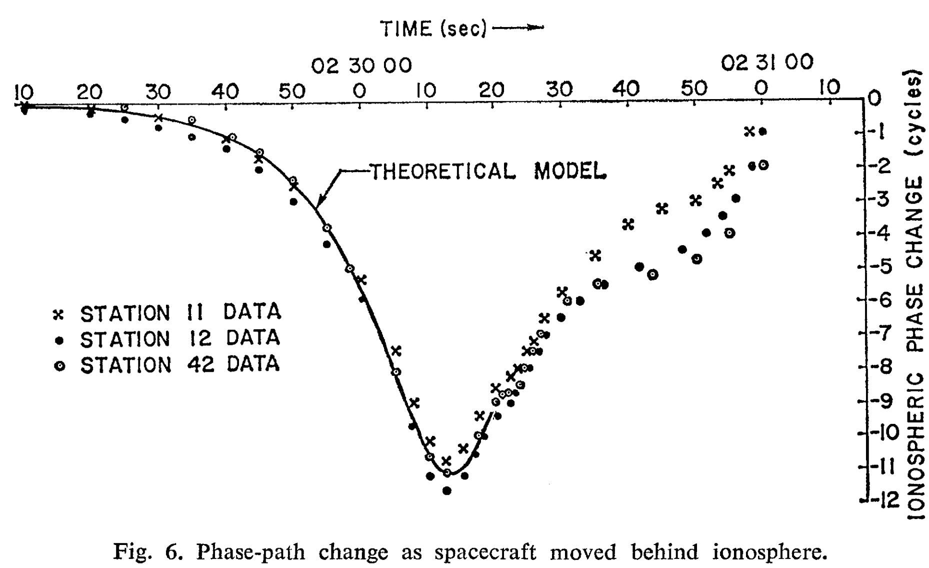

Fig. 6. Phase-path change as spacecraft moved behind ionosphere.

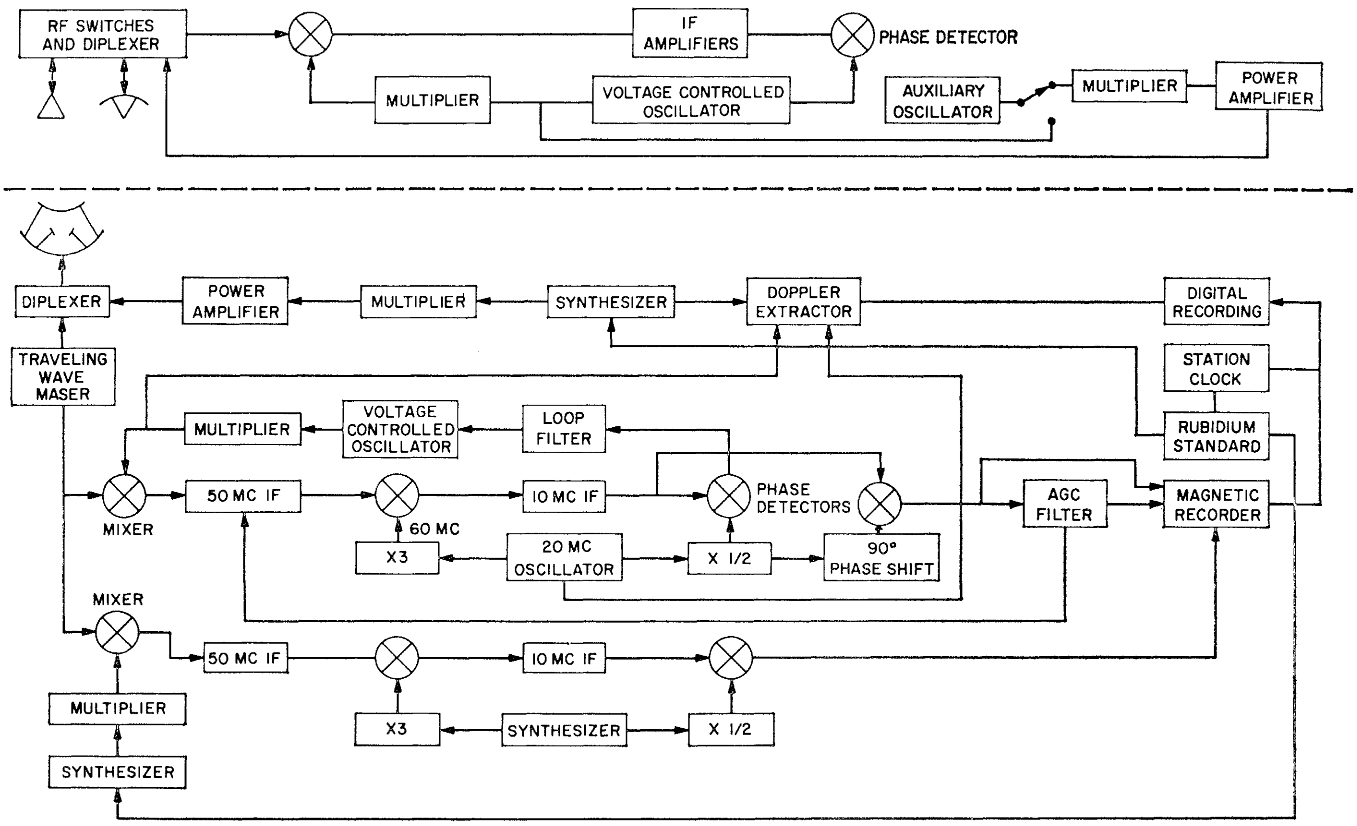

Fig. 7. Block diagram of DSIF radio system. MC, megacycles; X, times; IF, intermediate frequency; AGC, automatic gain control.

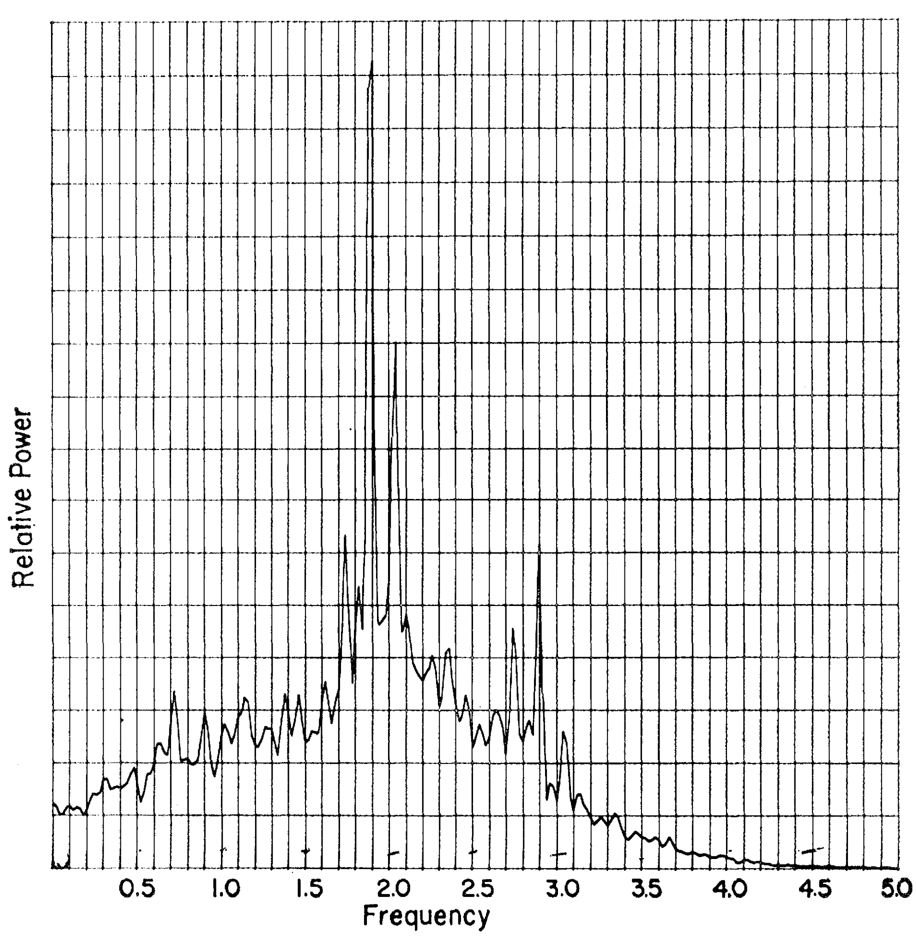

Fig. 8. Relative power spectral density. Frequency (abscissa) in kcy/sec.

of the other constituents, as well as the scale height, the temperature range is 175° ± 25°K, leading to a surface pressure of between 4.1 and 6.2 mb.

Finally, for the atmosphere having equal partial pressures of CO_2 and argon (model iii), the various properties are as follows: number density = $2.5 \pm 0.15 \times 10^{17}$ mol/cm^3; mass density = $1.75 \pm 0.1 \times 10^{-5}$ g/cm^3; temperature = 170° ± 20°K; and surface pressure = 5.0 to 7.0 mb.

The number densities derived for these models correspond to from 0.7 to 1.0 percent of the molecular number density of Earth's atmosphere at the surface. Since the scale height in the Martian atmosphere is apparently almost equal to that of Earth, the total number of molecules above a unit area on the surface of Mars is also on the order of 1 percent of that on Earth.

Figure 6 shows the change in two-way phase path as Mariner moved in behind the Martian ionosphere above Electris. Data from stations 11, 12, and 42 are all plotted in the same figure.

The local time was afternoon, and the sun was about 20 degrees above the horizon at the time when the S-band signal probed through this portion of the Martian atmosphere.

From the ionospheric phase-path data, one can determine the distribution in height of the electron density, $F(h)$. The electron-density profile may be calculated either from inversion of the integral equation relating the phase path to $F(h)$ or by curve-fitting or by both (*4–6*). A combination of these techniques is being used to determine the electron-density profile from the phase-path data.

Analysis of the data at this time indicates a distinct ionospheric layer with an electron-density peak of about 9×10^4 electrons per cubic centimeter (el/cm^3) at an altitude of about 125 km. The electron scale height above this peak is 20 to 25 km. (The neutral scale height is half this value.) The curve labeled "theoretical model" in Fig. 6 shows the phase path one would measure with this electron-density profile.

Both the small scale height above the electron-density peak and the low altitude of the peak, together with the small scale height in the neutral region near the surface, suggest that the Martian atmosphere is considerably cooler than previously anticipated.

The preliminary conclusion regarding the preponderance of CO_2 in the lower atmosphere also appears to be reasonably consistent with the ionospheric measurements, since high abundances of CO and O (resulting from the dissociation by solar radiation) indicate more effective radiative cooling than previous estimates (based on N_2 as the main constituent) suggested for the upper atmosphere of Mars.

The phase path data shown in Fig. 6 were taken when the spacecraft entered occultation. A preliminary analysis of the data obtained during exit does not show a detectable ionosphere. Thus, the nighttime (solar zenith angle 106°) electron density over Mare Acidalium is lower than the daytime density by at least a factor of 20.

There is a suggestion of a minor peak at the height of about 95 km. The two layers may correspond to E and F regions in the Martian ionosphere. It is interesting to note, although no doubt a happenstance due to the mixture of widely varying conditions, that the main Martian layer is very similar in electron density, scale height, and altitude to the normal E region of Earth's ionosphere. The data from below the peak also show evidence of nonspherical symmetry, as would be expected from the variable illumination along the ray path. We believe the maximum number density given above is correct to about 10 percent.

The ionospheric profile does not differ markedly from that expected if there were a Chapman layer above the peak. If the profile follows the well-known variations for this simplified model, the peak density at a solar zenith angle 0° would be 1.5×10^5 el/cm^3, corresponding to a critical frequency of 3.5 Mcy/sec, as compared with 2.7 Mcy/sec at 70° zenith angle. The total ionospheric contents along a vertical column would be 5×10^{11} el/cm^2 at 70° and 7×10^{11} el/cm^2 at 0°. Corresponding daytime densities in Earth's ionosphere are on the order of 10^6 el/cm^3, and vertical contents are about 10^{13} el/cm^2 with very large diurnal, seasonal, latitudinal, and sunspot-cycle variations. Temperatures in Earth's main ionospheric layer are approximately an order of magnitude larger than in this Martian layer.

There still remains some possibility that more detailed studies of the phase path will show some ionization at greater heights. There is a slight suggestion of this in the preliminary data. However, the number density would be very low in such a layer, if it exists.

The near or complete absence of a static magnetic field on Mars has very interesting implications with regard to understanding the ionosphere and atmosphere of both Mars and Earth. For Mars, it means that one can better understand formation and loss mechanisms and better relate these to the physical characteristics of the atmosphere and ionosphere, since there are no complicating effects of such a field. For Earth, many ionospheric phenomena are still not well understood, often because of the complicating effects of the magnetic field in controlling incoming charged particles, in affecting ionospheric motions, in storing high-energy particles which may provide a heating and ionization source, in affecting and controlling small- and large-scale ionospheric irregularities, and in providing partial shielding from the solar wind. Results of studies of the Martian ionosphere should thus help in separating and understanding various phenomena in Earth's ionosphere.

The results described have been derived from frequency, phase, and amplitude measurements at the DSIF receiving stations during the occultation experiment. To better understand these measurements, it will be helpful to have a brief description of the DSIF radio system, including the special modifications for the experiment. The block diagram of the system is illustrated in Fig. 7.

The ground station uses a rubidium standard to drive a frequency synthesizer. Its output is then modulated, multiplied 96 times in frequency, amplified, and transmitted to the spacecraft at 2.1 Gcy/sec. When the spacecraft receiver is in lock with the ground-station signal, the down-link frequency is derived from the receiver's voltage-controlled oscillator (VCO), which is phase-locked to the

Table 1. Summary of occultation experiment.

Atmosphere	
Surface refractivity	3.6 ± 0.2 *N* units
Scale height	8 to 10 km
Surface number density	
100% CO_2	$1.9 \pm 0.1 \times 10^{17}$ mol/cm^3
Up to 20% A or N_2, or a mixture	$2.1 \pm 0.2 \times 10^{17}$ mol/cm^3
50% A	$2.5 \pm 0.15 \times 10^{17}$ mol/cm^3
Surface mass density	
100% CO_2	$1.43 \pm 0.1 \times 10^{-5}$ g/cm^3
Up to 20% A or N_2, or a mixture	$1.5 \pm 0.15 \times 10^{-5}$ g/cm^3
50% A	$1.75 \pm 0.10 \times 10^{-5}$ g/cm^3
Temperature	
100% CO_2	180 ± 20°K
Up to 20% A or N_2, or a mixture	175 ± 25°K
50% A	170 ± 20°K
Surface pressure	
100% CO_2	4.1 to 5.7 mb
Up to 20% A or N_2, or a mixture	4.1 to 6.2 mb
50% A	5.0 to 7.0 mb
Ionosphere	
Maximum electron density ($\chi = 70°$)	$9 \pm 1.0 \times 10^4$ el/cm^3
Altitude of maximum	120 to 125 km
Electron scale height above maximum	20 to 25 km
Temperature	< 200°K at 120 to 200 km

received up-link signal. When no up-link is received, however, the down-link frequency is derived from a free-running crystal oscillator in the spacecraft. The radio frequency signal is amplified and transmitted from a high-gain spacecraft antenna.

The ground transmitter and receiver system employs an 85-foot (26-m) parabolic antenna with a Cassegrainian simultaneous-lobing feed. A traveling-wave maser cooled by a closed-cycle helium refrigerator operating at 4.2°K is used for the receiver front end. After amplification by the maser, the signal is split into two separate receiver channels. The first channel consists of a triple-conversion phase-locked receiver. It is operated in the standard DSIF receiver configuration. This receiver's VCO is kept in phase synchronism with the received signal. By a series of frequency multiplications, divisions, and additions, the transmitter's exciter frequency is coherently compared to the receiver's VCO to obtain the two-way Doppler frequency. The receiver's automatic gain control (AGC), which is a received-signal power-level tracking servo, is used to determine received-power level. Appropriate AGC voltages were recorded on magnetic tape, and the Doppler count was digitized. This system yielded frequency information in real time. This channel is also used as the sum channel of the pointing system for the simultaneous-lobing antenna.

The second receiver channel—a manually tuned, constant-gain, triple-conversion superheterodyne—is operated in a nonstandard configuration. It amplifies and translates the down-link signal to the audiofrequency region of the spectrum and then records it on magnetic tape. The local-oscillator (LO) signals for this receiver were derived from the rubidium frequency standard, which drives a pair of synthesizers. The first LO frequency was periodically stepped to keep the signal in the receiver's passband. The second and third LO's were derived from the second synthesizer operating at 19.996 Mcy/sec. The output of the third mixer had a passband of 1 to 3 kcy/sec, which was recorded on magnetic tape. Since the LO frequencies are derived from the rubidium standard, the frequency integrity of the Doppler is maintained. The analog information on the magnetic tape was digitized after the mission for use in a digital computer.

Figure 8 is a power spectrum of the audio open-loop signal made from the digitized tape on an IBM 7094 computer. The time interval from 03:25:16 to 03:25:17 was chosen. During this second, the one-way frequency, which was first observed as the vehicle reappeared at 03:25:08, was switched off. (This signal component can be seen at 2900 cy/sec.) After the one-way signal disappeared, the two-way signal was recorded at an audio frequency of 1900 cy/sec. The phase modulation sidebands at ± 150 cy/sec can be seen on both signals.

It should again be pointed out that these numbers are the results of less than 1 month's analysis with relatively crude techniques. As the analysis proceeds, the results will be refined, taking into account additional data as well as more sophisticated theoretical investigations of the physical characteristics of the atmosphere and ionosphere.

ARVYDAS KLIORE
DAN L. CAIN, GERALD S. LEVY
Jet Propulsion Laboratory, California Institute of Technology, Pasadena

VON R. ESHLEMAN
GUNNAR FJELDBO
Center for Radar Astronomy, Stanford University, Stanford, California

FRANK D. DRAKE
Department of Astronomy, Cornell University, Ithaca, New York

References and Notes

1. A. J. Kliore, D. L. Cain, G. S. Levy, V. R. Eshleman, F. D. Drake, G. Fjeldbo, *Astronaut. Aeronaut.* 7, 72 (1965). The occultation experiment has been conducted by investigators at JPL, Stanford University, and Cornell University.
2. L. D. Kaplan, G. Munch, H. Spinrad, *Astrophys. J.* **139** (1964); G. P. Kuiper, Mars issue, *Comm. Lunar Planetary Lab.* **2**, 79 (1964), Univ. of Arizona.
3. R. B. Norton, *NASA TN-D-2333* (NASA Code AFSS-A, Washington, D.C., 1964).
4. A. Kliore, D. L. Cain, T. W. Hamilton, *J.P.L. Tech. Rept. No. 32-674* (Jet Propulsion Laboratory, Pasadena, Calif., 1964); G. Fjeldbo, *Final Report NSF G-21543, SU-SEL-64-025* (Stanford University, Stanford, Calif., 1964).
5. G. Fjeldbo and V. R. Eshleman, *J. Geophys. Res.*, **70**, 13 (1965).
6. G. Fjeldbo, V. R. Eshleman, O. K. Garriott, F. L. Smith, III, *ibid.*, p. 15.
7. We thank the Mariner Project and Deep Space Net personnel of JPL for their excellent performance in the preparation for the experiment and the acquisition of data. Also, special gratitude is due T. W. Hamilton of JPL and B. B. Lusignan of Stanford University for their many contributions to the success of the experiment. This paper presents the results of one phase of research carried out at the JPL, California Institute of Technology, under NASA contract NAS 7-100. The Stanford contribution was supported under NASA contracts NGR 05-020-065 and NsG-377.

23 August 1965

Heat Stabilities of Acid Phosphatases from Pinto Bean Leaves

Abstract. *Two acid phosphatases were demonstrable by polyacrylamide gel electrophoresis. They had different mobilities and different heat stabilities in 1.0*M *acetate buffer,* pH *5.2. Both phosphatases had the same electrophoretic mobility in tris buffer at* pH *7.5, gave one boundary in the analytical ultracentrifuge in tris or acetate buffer, and had the same sedimentation coefficient. The difference in these properties suggests an alteration in conformation of the proteins by the buffer systems.*

Newer techniques of protein chemistry, especially starch gel and polyacrylamide gel electrophoresis, have spurred the study of protein changes that occurr in plant and animal organs during disease or ontogeny. We have been studying acid phosphatase changes in bean leaves after removing the terminal buds. The heat stability of this enzyme was found useful in its characterization. These studies raised the possibility that there were two acid phosphatases which differed in their stability to heat. Heat stability studies also suggest the occurrence of multiple acid phosphatases in other tissues (*1*).

Acid phosphatase was extracted from bean leaves (*Phaseolus vulgaris* L. var. Pinto) and highly purified (*2*). A 1.0*M* acetate buffer, *p*H 5.2, was employed as the extraction medium and a freeze-thaw cycle, carried out at *p*H 5.2, was introduced before column chromatography on diethylaminoethyl cellulose at *p*H 7.5 in 0.01*M* tris (hydroxymethyl) aminomethane-HCl (tris) buffer. Enzyme activity was assayed by the method of Torriani (*3*) and protein was determined by the micro-Kjeldahl technique (*4*). The enzyme had a broad substrate range, *p*H optimum at 5.2, and hydrolysis of *p*-nitrophenylphosphate was noncompetitively inhibited by fluoride (*2*). Thus the enzyme is a typical type II phosphomonoesterase.

Loss in enzyme activity on heating in 1.0*M* acetate buffer, *p*H 5.2, is shown in Fig. 1. The initial decay in acetate buffer is approximately first order, but the drop in activity stops after 40 minutes, which suggests that two enzymes were present in the enzyme preparation, one of which was less heat